CrystEngComm

Accepted Manuscript

ROYAL SOCIETY OF CHEMISTRY

www.rsc.org/crystengcomm

Isopolymolybdate-induced organic-inorganic hybrid assemblies with copper ions and bichelate-bridging ligands

Xiu-Li Hao,[a,b] Yuan-Yuan Ma,[a] Yong-Hui Wang,[a] Hong-Ying Zang*[a] and Yang-Guang Li*[a]

Received (in XXX, XXX) Xth XXXXXXXXX 201X, Accepted Xth XXXXXXXXX 201X
First published on the web Xth XXXXXXXXX 201X
DOI: 10.1039/b000000x

The heptamolybdate $[NH_4]_6[Mo_7O_{24}]$, as a common polyoxometalate (POM) precursor with dynamic configuration transformation in aqueous solution by changing pH, has been introduced into the hydrothermal reaction system containing copper ions and bichelate-bridging ligands, leading to the isolation of seven new organic–inorganic hybrid compounds $[Cu^{I}_{2}Lo_{2}][Mo_{6}O_{19}]$ (**1**), $[Cu^{II}_{2}Lo_{2}][\beta\text{-}Mo_{8}O_{26}]\cdot 2H_{2}O$ (**2**), $[Cu^{II}_{4}Lo_{2}(pypz)_{4}][\alpha\text{-}Mo_{8}O_{26}]\cdot 3H_{2}O$ (**3**), $[Cu^{II}_{4}Lp_{4}(H_{2}O)_{4}][\alpha\text{-}Mo_{8}O_{26}][\beta\text{-}Mo_{8}O_{26}]\cdot 4H_{2}O$ **(4),** $[Cu^{I}_{4}Lp_{3}][\beta\text{-}Mo_{8}O_{26}]\cdot H_{2}O$ (**5**), $[Cu^{I}_{4}Lp_{4}][\alpha\text{-}Mo_{8}O_{26}]$ (**6**), and $[Cu^{I}_{2}Lp_{2}(Emim)_{2}][\beta\text{-}Mo_{8}O_{26}]$ (**7**) (bis(3-(2-pyridyl)pyrazole-1-ylmethyl)benzene = bppmb, L*o* = 1,2-bppmb, L*p* = 1,4-bppmb, pypz = 3-(2-pyridyl)pyrazole, Emim = 1-ethyl-3-methylimidazolium). All compounds were characterized by elemental analyses, IR spectra, TG analyses, powder X-ray diffraction and single-crystal X-ray diffraction analyses. The structural analyses show that the isopolymolybdate clusters act as a type of "molecular adapter", which modulate the coordination mode of metal-organic subunits, leading to a series of new metal-organic secondary building units, such as the "Möbius-Ring"-type binuclear unit, "S"-type binuclear unit, butterfly-type unit, helical chain and mesomeric helical chain. As a result, the POM anions and the metal-organic subunits have the suitable matching mode to form new hybrid self-assemblies. The photocatalytic properties of compounds **1–7** for the degradation of Rhodamine-B (RhB) under UV irradiation were investigated. All compounds showed good catalytic activity. Furthermore, the luminescent properties of compounds **1–7** have also been explored, indicating an organic ligand-based emission mode for all compounds.

Introduction

Polyoxometalates (POMs) have been on the stage reflecting the diverse nature of this family of inorganic clusters, which exhibit a variety of compositions, architectures as well as potential applications in catalysis, photochemistry, molecular electronics, medicine, *etc*.[1] During the process of constructing POM-based inorganic-organic hybrid materials, not only how POMs influence the function of the hybrid materials but also the relationship between the structures and properties are worthy investigating, which will provide reliable strategies to design and synthesize special POM-based hybrid materials.[2] According to the literature, even different charge of POM anions can cause transformation of a metal-organic unit, benefiting the assembly of new hybrid complexes.[3] We proposed that a dynamic configuration of POM anions, acting as a "molecular adapter", might adjust the coordination mode of metal-organic subunits, leading to more novel assembly products of POM-based metal-organic frameworks. The octamolybdate can be a good candidate due to the versatile isomers such as *α*, *β*, *γ*, *δ*, *ε*, *ζ*, *η* and *θ* evidenced in 1970.[4,5] More importantly, these isomers are easily transformed to each other under mild changes of the system.[4,5]

In the synthesis of inorganic-organic hybrid materials, the type of organic N-donor bridging ligands is one of the important factors because the neutral organic N-donor ligands have strong coordination interactions with TM ions, which can been extensively used for constructing the POM-based metal-organic hybrid compounds. In the literature, N-donor ligands are generally classified into two types, namely the chelate and bridging ligands.[3,4,6] The former ones possess the following advantages: (i) stronger coordination ability to transition metal (TM) ions than the bridging ligands with mono-dentate N-donor groups (for example the pyridine group); (ii) infinite coordination modes with TM ions, such as a $\{ML_2\}$ tetra-coordinated distorted tetrahedral geometry and a $\{ML_3\}$ hexa-coordinated octahedral geometry (L represents the bi-dentate chelate ligand), which is suitable for the synthesis of desirable complexes.[7] If a $-(CH_2)_n-$ spacer and/or rigid phenyl center is introduced between two chelate groups, a kind of organic chelate-bridging N-donor ligands can be produced and may show potential advantages to build new POM-based hybrid compounds with cage-like, helical, or even porous structural features.

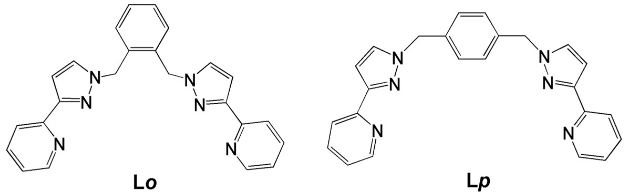

Scheme 1 The structural feature of the bichelate-bridging L*o* and L*p* ligands

Based on the aforementioned considerations, we chose a type of ligands combining both chelate and bridging functions, bis(3-(2-pyridyl)pyrazole-1-ylmethyl)benzene (abbr. bppmb) (as shown in Scheme 1), to explore new POM-based hybrid compounds.[8] We employed the Cu-bppmb coordination complexes and heptamolybdate as the POM precursor to in-situ synthesize seven new POM-based inorganic-organic hybrid compounds, $[Cu^{I}_{2}Lo_{2}][Mo_{6}O_{19}]$ (**1**), $[Cu^{II}_{2}Lo_{2}][\beta\text{-}Mo_{8}O_{26}]\cdot 2H_{2}O$ (**2**), $[Cu^{II}_{4}Lo_{2}(pypz)_{4}]$ $[\alpha\text{-}Mo_{8}O_{26}]\cdot 3H_{2}O$ (**3**), $[Cu^{II}_{4}Lp_{4}(H_{2}O)_{4}][\alpha\text{-}Mo_{8}O_{26}][\beta\text{-}Mo_{8}O_{26}]\cdot 4H_{2}O$ **(4),** $[Cu^{I}_{4}Lp_{3}][\beta\text{-}Mo_{8}O_{26}]\cdot H_{2}O$ (**5**) $[Cu^{I}_{4}Lp_{4}][\alpha\text{-}Mo_{8}O_{26}]$ (**6**), and $[Cu^{I}_{2}Lp_{2}(Emim)_{2}][\beta\text{-}Mo_{8}O_{26}]$ (**7**) (L*o* = 1,2-bppmb, L*p* = 1,4-bppmb, pypz = 3-(2-pyridyl)pyrazole, Emim = 1-ethyl-3-methylimidazolium). It is noteworthy that as the heptamolybdate in-situ transformed into hexamolybdate or different isomers of octamolybdates, the coordination modes of Cu-bppmb complex varied, leading to a series of new coordination units such as the “Möbius ring”-type binuclear unit, “S”-type binuclear unit, butterfly-type unit, chiral helical chain and mesomeric helical chain. The photocatalytic properties of compounds **1-7** have also been investigated.

Table 1. Crystal data and structure refinement for **1-7**.

Compounds	**1**	**2**	**3**	**4**
Formula	$C_{48}H_{40}N_{12}O_{19}Mo_6Cu_2$	$C_{48}H_{44}N_{12}O_{28}Mo_8Cu_2$	$C_{80}H_{70}N_{24}O_{29}Mo_8Cu_4$	$C_{96}H_{96}N_{24}O_{60}Mo_{16}Cu_4$
*M*r	1791.64	2131.55	2853.28	4335.17
T / K	150(2)	150(2)	150(2)	150(2)
Cryst. Syst.	Orthorhombic	Monoclinic	Monoclinic	Triclinic
Space group	*Pbcn*	$P2_1/c$	$P2_1/n$	*P-1*
a/Å	17.3590(6)	10.4332(2)	15.307(3)	14.8527(6)
b/Å	12.5591(4)	15.1148(3)	21.194(4)	15.7723(5)
c/Å	25.1230(7)	20.2219(5)	15.805(3)	17.4004(6)
α/°	90	90	90	72.343(3)
β/°	90	109.501(2)	10.53(3)	66.337(4)
γ/°	90	90	90	63.668(3)
V/Å^3	5477.2(3)	3005.98(11)	4801.5(17)	3306.9(2)
Z	4	2	2	1
μ / mm^{-1}	2.176	2.401	1.962	2.186
F(000)	3496	2068	2804	2108
Refls	19408	11421	36588	21482
R_{int}	0.0753	0.0255	0.0637	0.0710
GOF	0.987	1.022	1.020	1.008
R_1 $[I>2\sigma(I)]^a$	0.0438	0.0259	0.0417	0.0721
wR_2 (all data)^b	0.0861	0.0658	0.0910	0.1706
$\Delta\rho_{max,min}$/eÅ^{-3}	0.614 and -0.629	0.487 and -0.434	1.476 and -1.364	1.932 and -1.108

Compounds	**5**	**6**	**7**
Formula	$C_{72}H_{62}N_{18}O_{27}Mo_8Cu_4$	$C_{96}H_{80}N_{24}O_{26}Mo_8Cu_4$	$C_{60}H_{62}N_{16}O_{26}Mo_8Cu_2$
*M*r	2633.08	3007.52	2317.86
T / K	150(2)	150(2)	150(2)
Cryst. Syst.	Monoclinic	Triclinic	Monoclinic
Space group	*C2/c*	*P*-1	$P2_1/c$
a/Å	22.820(5)	13.7656(6)	14.4906(4)
b/Å	14.239(3)	14.8306(6)	13.7504(5)
c/Å	25.933(5)	16.0531(5)	18.9091(7)
α/°	90	117.470(3)	90
β/°	91.55(3)	109.431(3)	95.280(3)
γ/°	90	91.167(3)	90
V/Å^3	8424(3)	2682.32(18)	3751.7(2)
Z	4	1	2
μ / mm^{-1}	2.223	1.759	1.932
F(000)	5152	1484	2272
Refls	28518	16486	14215
R_{int}	0.1156	0.0503	0.0523
GOF	1.017	0.957	0.959
R_1 $[I>2\sigma(I)]^a$	0.0608	0.0586	0.0422
wR_2 (all data)^b	0.1326	0.1471	0.6335
$\Delta\rho_{max,min}$/eÅ^{-3}	0.537 and -0.568	1.037 and -0.665	1.076 and -0.693

Note: $^aR_1 = \Sigma||F_o| - |F_c||/\Sigma|F_o|$; $^bwR_2 = \Sigma[w(F_o^2 - F_c^2)^2]/\Sigma[w(F_o^2)^2]^{1/2}$.

Experimental

Materials and physical measurements

All reagents and solvents for the synthesis were purchased without further purification. The bichelate-bridging ligands L*o* and L*p* were prepared according to literature methods.[9] Elemental analyses (C, H and N) were carried out on a Perkin-Elmer 2400 CHN elemental analyzer. The FT-IR spectra were performed on a

Mattson Alpha-Centauri spectrometer with KBr pellets in the range of 4000 – 400 $\mathrm{cm^{-1}}$. TG analyses were performed on a Pyris Diamond TG instrument in flowing N_2 with a heating rate of 10 °C·$\mathrm{min^{-1}}$. The powder X-ray diffraction (PXRD) patterns were obtained with a Rigaku D/max-IIB X-ray diffractometer at a scanning rate of 1° per minute with 2θ ranging from 5° to 50° using Cu Kα radiation (λ = 1.5418 Å). Photocatalytic experiments in aqueous solutions were accomplished in a 500 mL water-cooled quartz cylindrical container. Usually, the reaction mixture in the container was kept at room temperature by a continuous flow of water through an external cooling coil. Moreover, a 125 W high-pressure mercury lamp was employed as the UV light source. A suspension of powdered catalyst (50 mg) in fresh aqueous solutions of Rhodamine-B (RhB) (400 mL, 20.0 mg·$\mathrm{L^{-1}}$) was magnetically stirred in the container in the dark for 30 min before irradiation in order to establish an adsorption/desorption equilibrium of RhB on the sample surface. At given 15-min irradiation intervals, 3 mL of samples were taken out from the beaker and subsequently analyzed by an SP-1900 UV−vis spectrophotometer. The organic dye concentration was estimated by the absorbance at 550 nm.

Synthesis

$[\mathrm{Cu^{I}_{2}L}o_{2}][\mathrm{Mo_6O_{19}}]$ **(1)**

A reaction mixture of $(\mathrm{NH_4})_6\mathrm{Mo_7O_{24}}\cdot 4\mathrm{H_2O}$ (0.16 g, 0.13 mmol), $\mathrm{CuCl_2}\cdot 2\mathrm{H_2O}$ (0.15 g, 0.87 mmol), L*o* (0.1 g, 0.25 mmol) and distilled water (10 mL) was stirred for 0.5 h at room temperature and adjusted to pH 2.0 with HCl (2 M). Then, the suspension was sealed into a Teflon-lined autoclave and kept under autogenous pressure at 180 °C for 5 days. After the autoclave was slowly cooled to room temperature at a rate of 10 °C·$\mathrm{h^{-1}}$, yellow block crystals were filtered and washed with distilled water (70% yield based on Mo). Anal. Calcd for $\mathrm{C_{48}H_{40}N_{12}O_{19}Mo_6Cu_2}$: C 32.15, H 2.23, N 9.38. Found: C 32.47, H 2.15, N 9.65. Selected IR (KBr pellet, $\mathrm{cm^{-1}}$): 3442(s), 3149(w), 3108(w), 1645(w), 1604(m), 1560(w), 1502(s), 1436(s), 1363(s), 1232(s), 1095(w), 1063(m), 955(s), 870(w), 800(s).

$[\mathrm{Cu^{II}_{2}L}o_{2}][\beta\text{-}\mathrm{Mo_8O_{26}}]\cdot 2\mathrm{H_2O}$ **(2)**

A reaction mixture of $(\mathrm{NH_4})_6\mathrm{Mo_7O_{24}}\cdot 4\mathrm{H_2O}$ (0.16 g, 0.13 mmol), $\mathrm{Cu(NO_3)_2}\cdot 3\mathrm{H_2O}$ (0.21 g, 0.87 mmol), L*o* (0.1 g, 0.25 mmol) and distilled water (10 mL) was stirred for 0.5 h at room temperature and adjusted to pH 4.5 with HCl (2 M). Then, the suspension was sealed into a Teflon-lined autoclave and kept under autogenous pressure at 180 °C for 5 days. After the autoclave was slowly cooled to room temperature at a rate of 10 °C·$\mathrm{h^{-1}}$, green block crystals were filtered and washed with distilled water (60% yield based on Mo). Anal. Calcd for $\mathrm{C_{48}H_{44}N_{12}O_{28}Mo_8Cu_2}$: C 27.02, H 2.06, N 7.88. Found: C 27.32, H 2.15, N 7.58. Selected IR (KBr pellet, $\mathrm{cm^{-1}}$): 3439(s), 3106(w), 1639(s), 1504(w), 1443(s), 1381(w), 1344(w), 1230(m), 1074(w), 953s), 891(s), 822(s), 773(w), 715(m), 660(w).

$[\mathrm{Cu^{I}_{4}L}o_{2}(\mathrm{pypz})_4][\alpha\text{-}\mathrm{Mo_8O_{26}}]\cdot 3\mathrm{H_2O}$ **(3)**

A reaction mixture of $(\mathrm{NH_4})_6\mathrm{Mo_7O_{24}}\cdot 4\mathrm{H_2O}$ (0.16 g, 0.13 mmol), $\mathrm{CuCl_2}\cdot 2\mathrm{H_2O}$ (0.15 g, 0.87 mmol), L*o* (0.1 g, 0.25 mmol), pypz (0.036 g, 0.25 mmol) and distilled water (10 mL) was stirred for 0.5 h at room temperature and adjusted to pH 3.0 with HCl (2 M). Then, the suspension was sealed into a Teflon-lined autoclave and kept under autogenous pressure at 180 °C for 5 days. After the autoclave was slowly cooled to room temperature at a rate of 10 °C·$\mathrm{h^{-1}}$, green block crystals were filtered and washed with distilled water (40% yield based on Mo). Anal. Calcd for $\mathrm{C_{80}H_{70}N_{24}O_{29}Mo_8Cu_4}$: C 33.65, H 2.45, N 11.78. Found: C 33.97, H 2.53, N 11.55. Selected IR (KBr pellet, $\mathrm{cm^{-1}}$): 3109(m), 1604(m), 1566(w), 1437(s), 1365(m), 1232(m), 1153(m), 1090(m), 939(s), 908(s), 850(s), 777(m), 715(s), 673(w).

$[\mathrm{Cu^{II}_{4}L}p_{4}(\mathrm{H_2O})_4][\alpha\text{-}\mathrm{Mo_8O_{26}}][\beta\text{-}\mathrm{Mo_8O_{26}}]\cdot 4\mathrm{H_2O}$ **(4)**

A mixture of $(\mathrm{NH_4})_6\mathrm{Mo_7O_{24}}\cdot 4\mathrm{H_2O}$ (0.16 g, 0.13 mmol), $\mathrm{CuCl_2}\cdot 2\mathrm{H_2O}$ (0.15 g, 0.87 mmol) and L*p* (0.1 g, 0.25 mmol), was dissolved in 10 mL of distilled water and adjusted to pH 3.7 with HCl (2 M) and NaOH (1 M). The mixture was stirred for 0.5h at room temperature. Then, the suspension was sealed into a Teflon-lined autoclave and kept under autogenous pressure at 180 °C for 5 days. After the autoclave was slowly cooled to room temperature at a rate of 10 °C·$\mathrm{h^{-1}}$, green block crystals were filtered and washed with distilled water (40% yield based on Mo). Anal. Calcd for $\mathrm{C_{96}H_{96}N_{24}O_{60}Mo_{16}Cu_4}$: C 26.57, H 2.21, N 7.75. Found: C 26.85, H 2.15, N 7.90. Selected IR (KBr pellet, $\mathrm{cm^{-1}}$): 3437(s), 3118(w), 1614(s), 1566(w), 1504(w), 1490(w), 1439(s), 1363(m), 1230(m), 1165(w), 1101(w), 945(s), 912(s), 839(w), 779(s), 657(m).

$[\mathrm{Cu^{I}_{4}L}p_{3}][\beta\text{-}\mathrm{Mo_8O_{26}}]\cdot \mathrm{H_2O}$ **(5)**

A mixture of $(\mathrm{NH_4})_6\mathrm{Mo_7O_{24}}\cdot 4\mathrm{H_2O}$ (0.16 g, 0.13 mmol), $\mathrm{CuCl_2}\cdot 2\mathrm{H_2O}$ (0.15 g, 0.87 mmol) and L*p* (0.1 g, 0.25 mmol), was dissolved in 10 mL of distilled water and adjusted to ca. pH 4.5 with HCl (2 M) and NaOH (1 M). The mixture was stirred for 0.5 h at room temperature. Then the suspension was sealed into a Teflon-lined autoclave and kept under autogenous pressure at 180 °C for 5 days. After the autoclave was slowly cooled to room temperature at a rate of 10 °C·$\mathrm{h^{-1}}$, black block crystals were filtered and washed with distilled water (40% yield based on Mo). Anal. Calcd for $\mathrm{C_{72}H_{62}N_{18}O_{27}Mo_8Cu_4}$: C 32.81, H 2.35, N 9.57. Found: C 32.61, H 2.46, N 9.78. Selected IR (KBr pellet, $\mathrm{cm^{-1}}$): 3448(s), 3118(w), 1635(s), 1496(w), 1436(s), 1348(w), 1230(m), 1153(w), 1064(w), 944(w), 919(s), 887(w), 852(s), 765(m), 690(m), 642(w).

$[\mathrm{Cu^{I}_{4}L}p_{4}][\alpha\text{-}\mathrm{Mo_8O_{26}}]$ **(6)**

A mixture of $(\mathrm{NH_4})_6\mathrm{Mo_7O_{24}}\cdot 4\mathrm{H_2O}$ (0.16 g, 0.13 mmol), $\mathrm{CuCl_2}\cdot 2\mathrm{H_2O}$ (0.15 g, 0.87 mmol), L*p* (0.1 g, 0.25 mmol),was dissolved in 10 mL of distilled water and adjusted to ca. pH 3.0 with HCl (2 M) and NaOH (1 M). The mixture was stirred for 0.5 h at room temperature. Then, the suspension was sealed into a Teflon-lined autoclave and kept under autogenous pressure at 180 °C for 5 days. After the autoclave was slowly cooled to room temperature at a rate of 10 °C·$\mathrm{h^{-1}}$, yellow block crystals were filtered and washed with distilled water (45% yield based on Mo). Anal. Calcd for $\mathrm{C_{96}H_{80}N_{24}O_{26}Mo_8Cu_4}$: C 38.30, H 2.66, N 11.17. Found: C 38.62, H 2.74, N 11.36. Selected IR (KBr pellet, $\mathrm{cm^{-1}}$): 3363(w), 3109(m), 1601(s), 1562(w), 1497(m), 1435(s), 1348(m), 1234(s), 1155(w), 1066(m), 916(s), 862(m), 810(s), 769(m), 736(w), 659(s).

$[\mathrm{Cu^{I}_{2}L}p_{2}(\mathrm{Emim})_2][\beta\text{-}\mathrm{Mo_8O_{26}}]$ **(7)**

A mixture of $(\mathrm{NH_4})_6\mathrm{Mo_7O_{24}}\cdot 4\mathrm{H_2O}$ (0.16 g, 0.13 mmol), $\mathrm{CuCl_2}\cdot 2\mathrm{H_2O}$ (0.15 g, 0.87 mmol), L*p* (0.1 g, 0.25 mmol) and [Emim]Br (2 g, 4.6 mmol),was adjusted to pH 4.5 with HCl (2 M) and NaOH (1 M). The mixture was stirred for 0.5 h at room temperature. Then, the suspension was sealed into a Teflon-lined autoclave and kept under autogenous pressure at 180 °C for 5 days. After the autoclave was slowly cooled to room temperature at a rate of 10 °C·$\mathrm{h^{-1}}$, brown block crystals were filtered and washed with distilled water (55% yield based on Mo). Anal. Calcd for $\mathrm{C_{60}H_{62}N_{16}O_{26}Mo_8Cu_2}$: C 31.06, H 2.67, N 9.66. Found: C 31.37, H 2.59, N 9.43. Selected IR (KBr pellet, $\mathrm{cm^{-1}}$): 3440(s), 3113(w), 3082(m), 1637(w), 1600(m), 1560(w), 1494(w), 1434(s), 1350(m), 1234(s), 1163(s), 1095(w), 947(s), 912(s), 838(s), 784(m), 714(s), 714(s), 659(m).

X-ray crystallography

The crystallographic data of compounds **1-7** were collected at 150 K on the Rigaku R-axis Rapid IP diffractometer using graphite monochromatic Mo Kα radiation (λ = 0.71073 Å) and IP techniques. A multi-scan absorption correction was applied. The crystal data of **1-7** were solved by the direct method and refined by a full-matrix least-squares method on F^2 using the *SHELXTL-97* crystallographic software package.[10] All non-H atoms were refined anisotropically except the disordered solvent water molecules. H atoms on the C atoms were fixed in calculated positions. H atoms on the coordinated water molecules were found from the difference Fourier maps and fixed in reasonable positions. However, the H atoms on the lattice water molecules cannot be found from the residual peaks but were directly included in the final molecular formula. Furthermore, compound **2** exhibits solvent accessible voids in the final refinement but the residual peaks are too weak to be confirmed as solvent molecules. Based on the elemental analysis and TG analysis, the extra two solvent water molecules were directly included in the final molecular formula of **2**. The detailed crystal data and structure refinement for **1**-**7** are given in Table 1. Selected bond lengths and angles of **1-7** are listed in Table S1- S7, respectively.

Results and Discussion

Crystal Structures

The POM anions existing in compound **1** are the classical Lindqvist-type polyoxoanions $[Mo_6O_{19}]^{2-}$, which are formed by six MoO_6 octahedra connected with each other through edge-sharing oxygen atoms and thus exhibit approximate O_h symmetry (Fig. S1a and d). The inorganic building blocks in compounds **2**–**7** are $[\alpha\text{-}Mo_8O_{26}]^{4-}$ (α-Mo$_8$), $[\beta\text{-}Mo_8O_{26}]^{4-}$ (β-Mo$_8$), or both ($[\alpha/\beta\text{-}Mo_8O_{26}]^{4-}$, α/β-Mo$_8$) anions. These polyoxoanions lie in the inversion centers. The α-Mo$_8$ anion consists of six distorted $\{MoO_6\}$ octahedra and two distorted $\{MoO_4\}$ tetrahedra with three kinds of O atoms, namely six μ_3-O, six μ-O, and fourteen terminal oxygen atoms (O_t) (Fig. S1b and e). The β-Mo$_8$ anion is composed of eight distorted $\{MoO_6\}$ octahedra with four kinds of O atoms, including six μ-O, four μ_3-O, two μ_5-O, and twelve O_t (Fig. S1c and f).

Structure description of 1

Single-crystal X-ray diffraction analysis shows that compound **1** crystallizes in the orthorhombic space group *Pbcn* and the basic structural unit consists of one cationic $[Cu^I_2(Lo)_2]^{2+}$ unit and one Lindqvist polyoxoanion $[Mo_6O_{19}]^{2-}$ (Fig. 1 and Fig S2). The $[Mo_6O_{19}]^{2-}$ moiety has crystallographically-imposed inversion symmetry, with O6 atom on an inversion centre. In the $[Cu^I_2(Lo)_2]^{2+}$ unit (Fig. 1a), each Cu^I center is four-coordinated with four N atoms derived from two different L*o* ligands and exhibits a distorted tetragonal coordination geometry. The bond lengths of Cu-N vary from 2.020(5) - 2.122(5) Å and the bond angles of N-Cu-N are in the range of 80.7(2) to 146.5(2)°. In this metal-organic unit, the L*o* ligand adopts an "*anti*"-style configuration and acts as a four-dentate chelate ligand to coordinate with two Cu centers to form the binuclear Cu-cluster (Fig. 1a). Such a moiety lies about a twofold axis. Furthermore, these cationic units are extended into 2D supramolecular sheets through $\pi\ldots\pi$ interactions with distances of 3.689(1) to 4.030(1) Å between the pyridyl rings and the pyrazole rings in the *ab* plane (Fig. 1c and Fig. S3). It is noteworthy that such 2D supramolecular sheets possesses honeycomb-like cavities, which are occupied by the $[Mo_6O_{19}]^{2-}$ POM units (Fig. 1c). Based on extensive weak $\pi\ldots\pi$ interactions in the structure, these $[Cu(I)_2(Lo)_2]^{2+}$ units form 2-D supramolecular sheets, which are well separated by the Lindqvist-type POM clusters, as shown in Fig. S4.

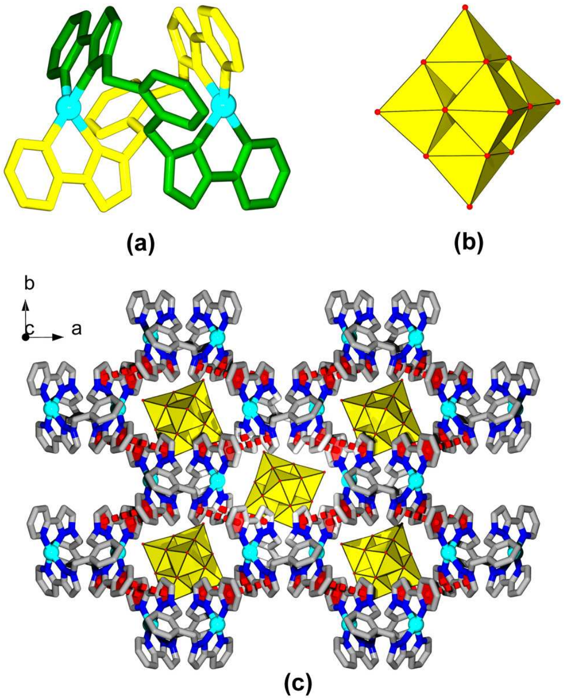

Figure 1 **(a)** Ball-and-stick view of binuclear $[Cu^I_2Lo_2]^{2+}$ unit in **1; (b)** Polyhedral view of $[Mo_6O_{19}]^{2-}$ cluster in **1; (c)** View of 2-D cationic supramolecular layer constructed by $\pi\ldots\pi$ interactions of adjacent binuclear $[Cu^I_2Lo_2]^{2+}$ units viewed along *c* axis in **1.** The cavities of the 2-D supramolecular layer are occupied by the POM anions

Structure description of 2

Single-crystal X-ray diffraction analysis indicates that compound **2** crystallizes in the monoclinic space group $P2_1$/c and consists of two $[Cu^{II}Lo]^{2+}$ moieties and one $[\beta\text{-}Mo_8O_{26}]^{4-}$ polyoxoanion (Fig. 2 and Fig. S5). In the crystal structure of **2**, the $[\beta\text{-}Mo_8O_{26}]^{4-}$ moiety lies about an inversion centre. Each L*o* ligand in **2** adopts a "*syn*"-style configuration, coordinating with one Cu^{II} center to form the mononuclear {CuL*o*} moiety (Fig. 2a). The two chelate bppmb groups in the [CuL*o*] unit are not in the same plane, but distort each other with a dihedral angel of 42.727(9)° (Fig. S6a). The Cu^{II} center is five-coordinated with four N atoms derived from the same L*o* ligand and one terminal O (O7) atom originating from the polyoxoanion, exhibiting a distorted tetragonal pyramid coordination geometry. The bond distances of Cu-N are in the range of 1.957(3)-2.140(3) Å and that of Cu-O is 2.063(2) Å. The bond angles of N–Cu–N range from 80.17(1) to 176.37(2)° and those of N–Cu–O from 88.51(1) to 135.07(1)°. Moreover, two mononuclear {CuL*o*} units are connected with the $[\beta\text{-}Mo_8O_{26}]^{4-}$ to form a {CuL*o*}-decorated POM cluster (Fig. 2c). Interestingly, the adjacent [CuL*o*] units are further connected into a 2-D supramolecular network in *bc* plane via weak intermolecular C-H…π interactions between the pyrazole/pyridine rings (Fig. S6b and Fig. S7). The typical C-H…π distances are 2.724(2) to 3.194(4) Å. In the packing arrangement, the 2-D supramolecular networks are well separated without obvious H-bonding or $\pi\ldots\pi$ interactions (Fig. S8).

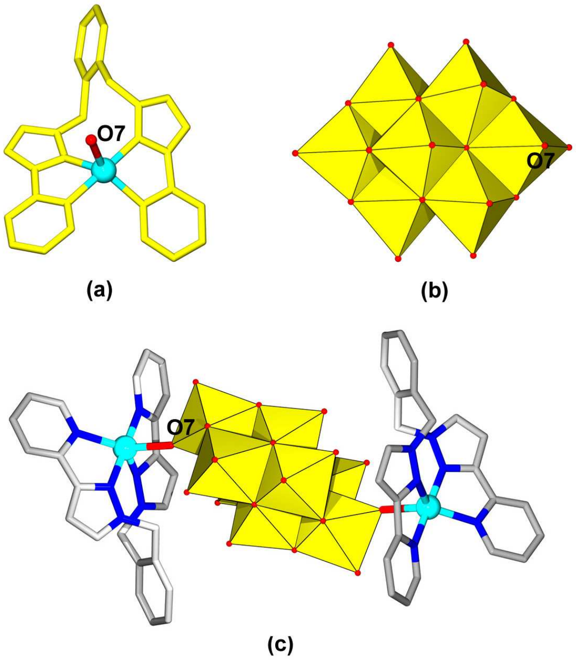

Figure 2 **(a)** Ball-and-stick view of [CuL*o*] fragment in **2**; (b) Polyhedral view of [*β*-Mo_8O_{26}]$^{4-}$ unit in **2**; (c) The [CuL*o*]-decorated POM hybrid cluster of **2**

Structure description of 3

Single-crystal X-ray diffraction analysis reveals that compound **3** crystallizes in the monoclinic space group $P2_1/n$, whose basic structural unit contains one polyoxoanion [α-Mo_8O_{26}]$^{4-}$ and two binuclear [Cu_2(pypz)$_2$(Lo)]$^{2+}$ units (Fig. 3 and Fig. S9). The [α-Mo_8O_{26}]$^{4-}$ moiety lies about an inversion centre in the crystal structure of **3**. In the binuclear [Cu_2(pypz)$_2$(Lo)]$^{2+}$ unit, there are two different Cu^{II} centers (Fig. 3a). The Cu(2) ion shows a five-coordinated environment with two nitrogen atoms derived from the L*o* ligand and three nitrogen atoms from two different pzpy ligands. Nevertheless, the Cu(1) ion possesses a six-coordinated environment, where it coordinates not only with five N atoms from the organic ligands (similar to the case of Cu(2)) but also with one terminal O atom from the polyoxoanion. The bond distances of Cu-N range from 1.955(5) to 2.312(5) Å and that of Cu-O is 2.594(0) Å. The bond angles of N-Cu-N range from 75.87(2) to 177.1(2)° and those of N–Cu–O from 81.7(8) to 169.0(5)°. Moreover, the two Cu centers are connected with each other via one L*o* ligand with "*syn*"-style configuration and two the pzpy ligands to form the binuclear Cu-cluste. It is noteworthy that the "*syn*"-style configuration of Lo ligand in compound **3** is different with those in compound **1** and **2**, indicating that the introduction of flexible –(CH_2)– spacers in L*o* ligand can provide various changes for the bridging ligand. The interesting structural feature of compound **3** is that two binuclear [Cu_2(pypz)$_2$(Lo)]$^{2+}$ units are connected with one [α-Mo_8O_{26}]$^{4-}$ moiety, forming a dumbbell-like hybrid cluster (Fig. 3c). In the packing arrangement, these hybrid clusters possess two kinds of orientations, but no obvious intermolecular interactions among the adjacent molecules in the packing arrangement of **3** (Fig. S10).

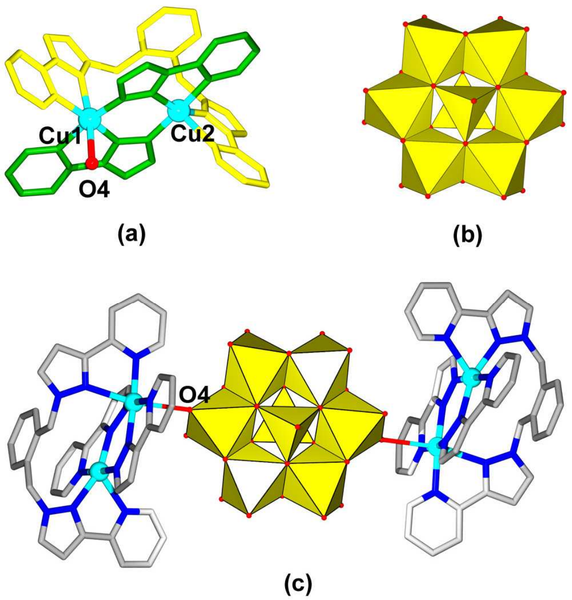

Figure 3 **(a)** Ball-and-stick view of binuclear [Cu_2(pypz)$_2$L*o*] moiety in **3**; **(b)** Polyhedral view of [α-Mo_8O_{26}]$^{4-}$ unit in **3**; **(c)** The [Cu_2(pypz)$_2$L*o*]-decorated POM hybrid cluster of **3**

Structure description of 4

Single-crystal X-ray diffraction analysis displays that compound **4** crystallizes in the triclinic space group *P*-1. The basic structural unit of **4** consists of one [α-Mo_8O_{26}]$^{4-}$ anion, one [β-Mo_8O_{26}]$^{4-}$ anion, and two cationic binuclear [$Cu^{II}_2Lp_2(H_2O)_2$]$^{4+}$ moieties (Fig. 4 and Fig. S11). It is noteworthy that the [α-Mo_8O_{26}]$^{4-}$ and [β-Mo_8O_{26}]$^{4-}$ moieties each lies about an inversion centre in the crystal structure of **4**. In **4**, all Cu^{II} ions adopt the six-coordinated environment with four nitrogen atoms derived from two different L*p* ligands, one oxygen atom from the polyoxoanion, and one coordinated water molecule (Fig. 4a). The bond distances of Cu-N are in the range of 1.956(9) - 2.355(1) Å and those of Cu-O vary from 2.029(8) to 2.479(7) Å. The bond angles of N-Cu-N range from 76.7(4) to 179.9(5)° and the N-Cu-O angles are in the range of 80.3(3)-167.3(1)°. Moreover, each Cu(1) ion is connected with one Cu(2) ion by two L*p* ligands with the *cis*-configuration to form a chiral "Möbius-Ring (MR)"-type binuclear moiety.

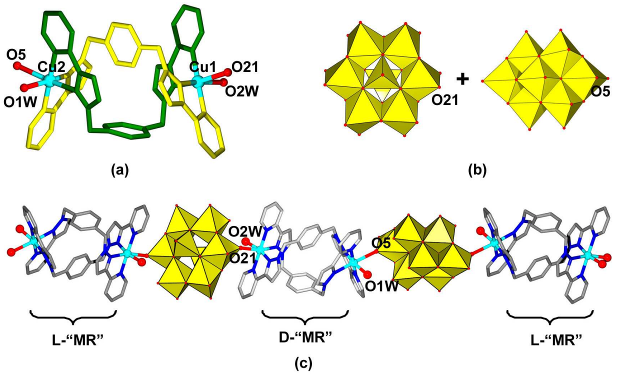

Figure 4 **(a)** Ball-and-stick view of binuclear [$Cu_2Lp_2(H_2O)_2$]$^{4+}$ unit in **4,** showing the "Möbius-Ring (MR)"-type structural feature; (b) Polyhedral view of both [α-Mo_8O_{26}]$^{4-}$ and [β-Mo_8O_{26}]$^{4-}$ anionic clusters in **4**; (c) The 1-D chainlike hybrid compound of **4** composed of binuclear [$Cu_2Lp_2(H_2O)_2$]$^{4+}$ unit, (α-Mo_8O_{26})$^{4-}$ anions and (β-Mo_8O_{26})$^{4-}$ anions.

More interestingly, such a chiral binuclear metal-organic unit is connect with a centrosymmetric $[\alpha\text{-Mo}_8\text{O}_{26}]^{4-}$ anion via the Cu(1) center on one side and linked with a centrosymmetric $[\beta\text{-Mo}_8\text{O}_{26}]^{4-}$ anion via the Cu(2) center on the other side, forming a 1-D chainlike hybrid compound. (Fig. 4c). It is worth noting that the left-handed and right-handed "MR"-type moieties are alternatively arranged in the chain, leading to a mesomeric chain (Fig. 4c). To our knowledge, such a hybrid chain composed of both $[\alpha\text{-Mo}_8\text{O}_{26}]^{4-}$ and $[\beta\text{-Mo}_8\text{O}_{26}]^{4-}$ units is observed for the first time. In the packing arrangement, all the 1-D chains are parallel with each other and well separated in three dimensions without obvious intermolecular interactions (Fig. S12).

Structure description of 5

Single-crystal X-ray diffraction analysis reveals that compound **5** crystallizes in the monoclinic space group *C*2/c. The structure contains two types of chainlike building units. One is composed of $[\beta\text{-Mo}_8\text{O}_{26}]^{4-}$ polyoxoanion and a binuclear $[\text{Cu}_2\text{L}p]^{2+}$ metal-organic bridging fragment (labeled with **Chain I**), in which $[\beta\text{-Mo}_8\text{O}_{26}]$ moiety lies about an inversion centre in the crystal structure of **5**, while the L*p* ligand lies about another independent inversion centre. The other is a $[\text{Cu}_2\text{L}p_2]^{2+}$ metal-organic chainlike moiety (labeled with **Chain II**) (Fig. 5). In **5**, each Cu(1) center is four-coordinated with two N atoms derived from the L*p* ligand and two oxygen atoms from the polyoxoanion (Fig. 5a). The bond distances of Cu-N are 2.004(1) and 2.106(9) Å and those of Cu-O are 1.929(6) and 2.063(7) Å, respectively. The bond angle of N-Cu-N is 81.4(4)° and N-Cu-O are in the range of 92.7(3)-136.8(3)°. Two of such Cu(1) ions are connected with each other by one L*p* ligand with the "*anti*"-configuration to form a $\{\text{Cu}_2\text{L}p\}$ binuclear fragment. Interestingly, these $\{\text{Cu}_2\text{L}p\}$ fragments are further linked by the $[\beta\text{-Mo}_8\text{O}_{26}]^{4-}$ polyoxoanions into a "zig-zag"-type chain (**Chain I**) (Fig. 5c). Each Cu(2) center also exhibits the tetra-coordinated environment, whereas it is coordinated with four N atoms from two different L*p* ligands (Fig. 5c). The Cu-N bond distances are in the range of 1.976(8) - 2.107(1) Å and the N-Cu-N bond angles vary from 80.4(3) to 132.5(4)°. Interestingly, the neighboring Cu(2) centers are connected by the L*p* ligands with the "*anti*"-configuration into a 1-D $\{\text{Cu}_2\text{L}p_2\}$ chain (**Chain II**) (Fig. 5d).

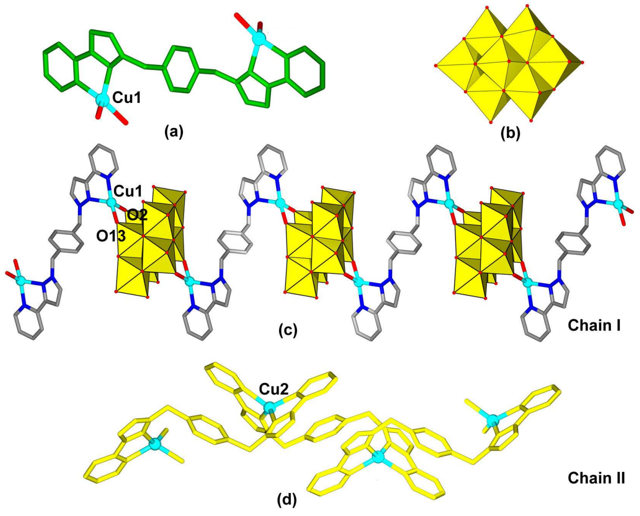

Figure 5 **(a)** Ball-and-stick view of binuclear $[\text{Cu}^{\text{I}}_2\text{L}p]$ bridging unit in **5**; **(b)** The polyhedral view of $[\beta\text{-Mo}_8\text{O}_{26}]^{4-}$ anionic cluster in **5;** **(c)** The structure of 1-D hybrid **Chain I** composed of the $[\text{Cu}^{\text{I}}_2\text{L}p]$ and $[\beta\text{-Mo}_8\text{O}_{26}]^{4-}$ units; **(d)** The other $[\text{Cu}_2\text{L}p_2]$ metal-organic **Chain II** in **5**.

Although both L*p* ligands in **5** exhibit the "*anti*"-configuration, the distances between two Cu^{I} centers are 9.523(9) and 7.639(4) Å, respectively(Fig. S14), indicating that the L*p* ligands in two types of chains possess different "*anti*"-configurations. Furthermore, the $[\text{Cu}_2\text{L}p_2]^{2+}$ metal-organic **Chain II** displays a chiral helical feature. Both left-handed and right-handed helical chains can be observed along *a* axis (Fig. 6b). In the packing arrangement, all the chains are parallel with each other on *ab* plane (Fig. 6 and Fig. S13). It is noteworthy that **Chain I** shows two kinds of orientation in the crystal structure, and such two different **Chain Is** are separated by the supramolecular layer composed of **Chains II** (Fig. 6 and Fig. S15). Furthermore, all left-handed helical chains are parallel with each other on one layer of *ab* plane, while all right-handed helical chains are parallel with each other on the other layer of *ab* plane (Fig. 6c). The two types of layers are alternately arranged along *c* axis, leading to a racemic **compound 5**. In the packing arrangement, all these chains are stacked together by weak C-H…π intermolecular interactions between the benzene rings of two neighboring chains (Fig. S15d).

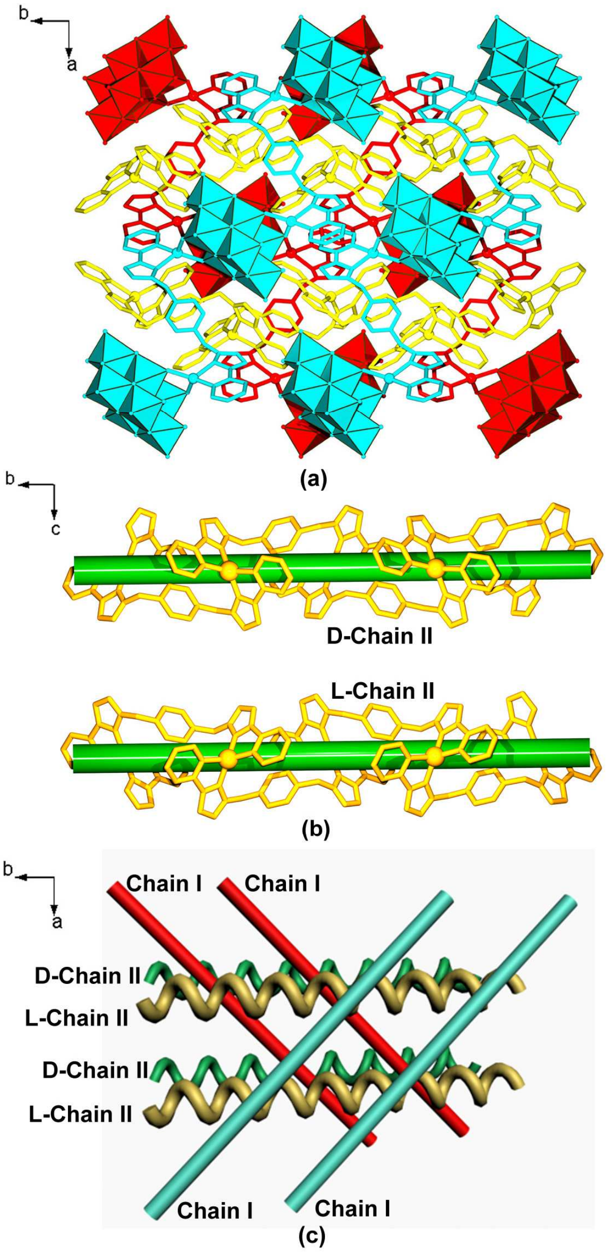

Figure 6 (**a**) Packing arrangement of compound **5** viewed along *c* axis; The chains in different layers are shown with blue, yellow and red colors; (b) The left-handed and right-handed helical **Chain II**s (labeled with L-Chain II and D-Chain II) in **5**; (**c**) Schematic view of the packing mode of various chains in **5**.

Structure description of 6

Single-crystal X-ray diffraction analysis displays that compound **6** crystallizes in the triclinic space group *P*-1. The basic structural unit contains one $[\alpha\text{-}Mo_8O_{26}]^{4-}$ polyoxoanion and two types of 1-D $[Cu^{I}_{2}Lp_{2}]^{2+}$ metal-organic chains (Fig. 7 and Fig S16). It is worth mentioning that all three components lie about independent inversion centres. In **6**, one type of $[Cu^{I}_{2}Lp_{2}]^{2+}$ chain is formed via alternate linking of the "*anti*"-style L*p* ligands by Cu(1) centers along *c* axis (Fig. 7a), where the Cu(1) centers exhibit the tetra-coordinated environment with four N atoms derived from two different L*p* ligands. The bond distances of Cu-N vary from 2.023(7) to 2.086(7) Å and the bond angles of N-Cu-N from 77.4(3) to 145.8(3)°. Moreover, the L*p* ligands show two types of configuration, namely Lp^1 and Lp^2, and the distances between two Cu(1) centers in Lp^1 and Lp^2 are 8.444(2) Å and 9.660(5) Å, respectively (Fig. S17a-b). In contrast, the alternate connection of the "*anti*"-style L*p* ligands with Cu(2) centers results in the other type of $[Cu^{I}_{2}Lp_{2}]^{2+}$ chain along *a* axis (Fig. 7b). The L*p* ligands also display two types of configuration, that is, Lp^3 and Lp^4 (Fig. S17c-d). The distances between two Cu(2) centers in Lp^3 and Lp^4 are 8.152(8) and 11.008(1) Å, respectively (Fig. S4c and S4d). It is worth mentioning that both chains in compound **6** are not chiral helical chains, but show a mesomeric helical topology. In such mesomeric chain, the left-handed helical unit and the right-handed helical unit are alternately connected together, leading to a mesomeric feature.[9,12] In the packing arrangement, The chains along *c* axis and the those along *a* axis are stacked together, forming a 3-D supramolecular open framework (Fig. 8). The adjacent chains are stabilized by the π…π intermolecular interactions between benzene rings from different chains. The typical distance between two adjacent benzene planes is ca. 3.487(1) Å (Fig. S18). The $[\alpha\text{-}Mo_8O_{26}]^{4-}$ polyoxoanions reside in the cavities as the guest templates (Fig. 8a).

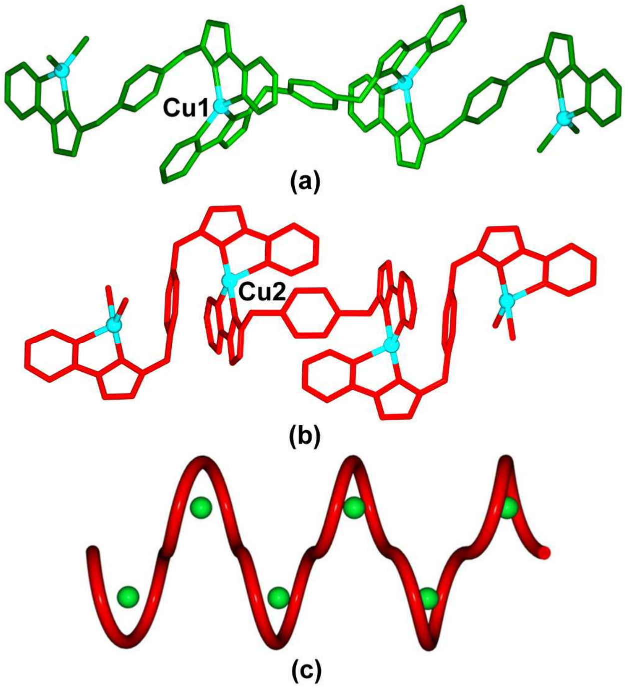

Figure 7 (**a**) The structure of the $[Cu(1)_2Lp_2]^{2+}$ chain in **6**; (**b**) The structure of the $[Cu(2)_2Lp_2]^{2+}$ chain in **6**; (c) Schematic view of the mesomeric helical structural feature of both chain in **6** (The green balls represent Cu center).

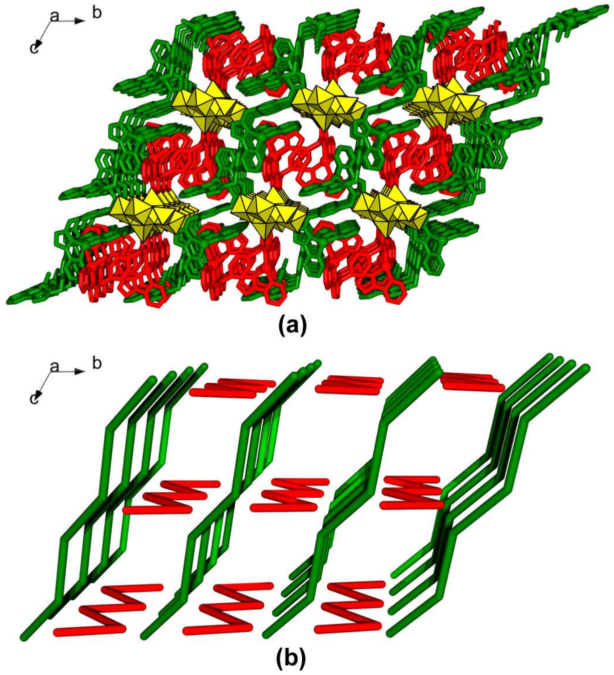

Figure 8 (**a**) Packing arrangement of **compound 6** viewed along *a* axis; Two types of 1-D chains are shown with green and red color, respectively; (**b**) Schematic view of the 3-D supramolecular framework of **6** view along *a* axis; The 1-D chains are simplified with the zig-zag lines. The POMs in the cavities are omitted for clarity.

Structure description of 7

Single-crystal X-ray diffraction analysis displays that compound **7** crystallizes in the monoclinic space group $P2_1/c$, whose basic structural unit consists of one cationic $[Cu^{I}_{2}Lp_{2}]^{2+}$ metal-organic chain, one $[\beta\text{-}Mo_8O_{26}]^{4-}$ polyoxoanion and two $[Emim]^+$ cations (Fig. 9 and Fig. S20). In the crystal structure of **7**, $[\beta\text{-}Mo_8O_{26}]$ moiety lies about an inversion centre. In the $[Cu^{I}_{2}Lp_{2}]^{2+}$ chain of **7**, each Cu(I) cation adopts a four-coordinated mode with four nitrogen atoms derived from two different L*p* ligands (Fig. 9c). The bond distances of Cu-N vary from 2.006(7)-2.113(7)Å, and the bond angles of N-Cu-N are in the range of 79.4(3)° to 136.7(3)°. Interestingly, each L*p* ligand in 7 adopts the similar trans-configuration, which is linked by two Cu(I) centers to form the 1-D helical chain. Furthermore, there are extensive C-H…π intermolecular interactions between the adjacent left-handed and right-handed helical chains in *bc* plane, forming 2-D supramolecular layer (Fig. 10 and Fig. S16). In the packing arrangement, all these 2-D supramolecular layers are parallel with each other and are well separated by the $[Emim]^+$ cations and the $[\beta\text{-}Mo_8O_{26}]^{4-}$ polyoxoanions (Fig. 11 and Fig. S21).

During the synthesis in Cu(I)/BBTZ/POM reaction system, it is worth emphasizing the design and use of two initial reaction materials. The first important precursor is the Cu(I) ion. As the linking nodes in the final structural frameworks, Cu(I) ions are originated from the reduction of Cu(II) ions by the organic N-donor ligands in the hydrothermal environment.[5d] Interestingly, such in situ obtained Cu(I) ions seem to be more active than the Cu(I)Cl precursors to coordinate with organic N-donor ligands, since no crystalline compounds were obtained when Cu(II) ions were substituted by CuCl in the initial reaction materials. Another important precursor is the Keggin-type POMs with different negative charges. Usually, the charge can be modulated by the change of the central hetero-atoms of the POMs. With this strategy, we selected a series of Keggin-type polyoxoanions with different negative charges, such as $[PMo_{12}O_{40}]^{3-}$, $[SiMo_{12}O_{40}]^{4-}$ and $[BW_{12}O_{40}]^{5-}$. Another way is to introduce different numbers of low-valent metal centers into the POM clusters, exemplified by the $[PMo_{10}V_2O_{40}]^{5-}$ and $[PMo_9V_3O_{40}]^{6-}$. The third route is to reduce the POMs into heteropoly-blue with relatively strong reductants. In our work, the hexamethylenetetramine was employed to reduce $[SiW_{12}O_{40}]^{4-}$ into $[SiW^{V}_2W^{VI}_{10}O_{40}]^{6-}$ in the hydrothermal conditions. By the use of all above Keggin-type polyoxoanions, three new POM-based inorganic-organic hybrid compounds of good single-crystal quality were obtained. No crystalline compounds with $[BW_{12}O_{40}]^{5-}$, $[PMo_{10}V_2O_{40}]^{5-}$ and $[PMo_9V_3O_{40}]^{6-}$ POMs have been isolated yet.

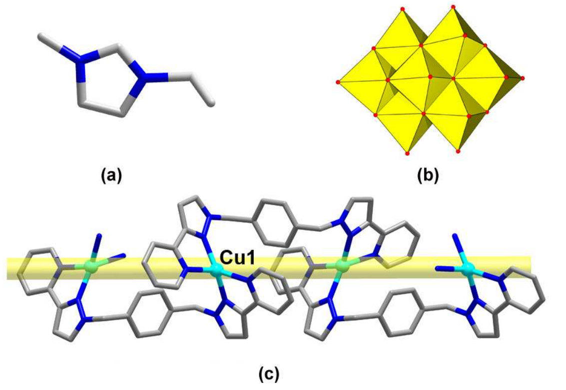

Figure 9 **(a)** The structure of $[Emim]^+$ cation in 7; **(b)** The structure of $[\beta\text{-}Mo_8O_{26}]^{4-}$ polyoxoanion cluster in **7; (c)** The helical $[Cu^{I}_2Lp_2]^{2+}$ chain in **7.**

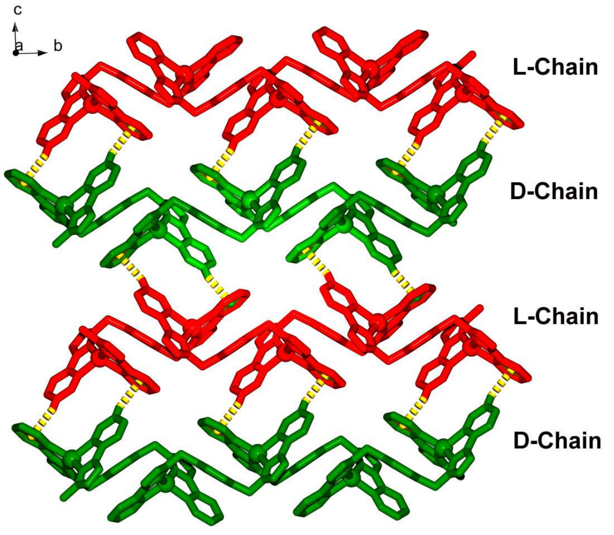

Figure 10 The 2-D supramolecular layer in **7** formed by left-handed and right-handed helical chains (labeled with **L-** and **D-Chain**) via the C-H…π intermolecular interactions in *bc* plane.

Synthetic and structural discussion

In the system containing chelating-bridging ligands, copper ions and heptamolybdate, the heptamolybdate $[Mo_7O_{24}]^{6-}$ can *in situ* transform to hexamolybdate or octamolybdate by changing pH of the system. By comparing these seven compounds, at distinct pH value range, heptamolybdate preferred to form different form of isopolyoxomolybdate: in the range of pH< 2, the $[Mo_6O_{19}]^{2-}$ anion was predominant; at pH 3.0, the $[\alpha\text{-}Mo_8O_{26}]^{4-}$ anion was the main form; pH= 3.5-4.0, $[\alpha\text{-}Mo_8O_{26}]^{4-}$ and $[\beta\text{-}Mo_8O_{26}]^{4-}$ coexist at the same time; pH> 4.0, heptamolybdate transformed to $[\beta\text{-}Mo_8O_{26}]^{4-}$ isomer. The slight change of pH led to different forms of isopolyoxomolybdate and different forms of isopolyoxoanions influenced the assembly of the metal-organic subunits. Additionally, The different coordination ability of surface oxygen atoms on different POMs induced distinct interaction modes between POMs and metal-organic subunits so as to obtain multiple self-assembled POM-based inorganic-organic hybrid materials. In this investigation, different forms of isopolyoxomolybdates can be viewed as a "molecular adaptor" to tune the appropriate form of metal-organic subunits so that the POM anions and the metal-organic subunits have the best matching mode in the self-assembly process (Scheme 2). This may offer a new approach to construct a series of POM directed metal-organic hybrid materials.

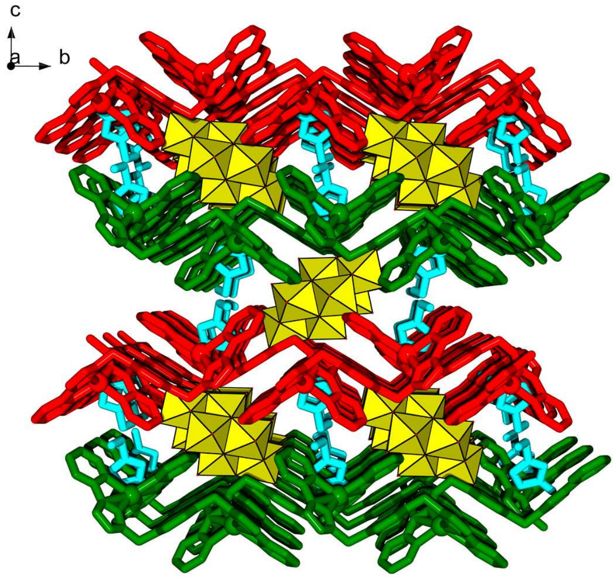

Figure 11 Packing arrangement of **compound 7** viewed along *a* axis.

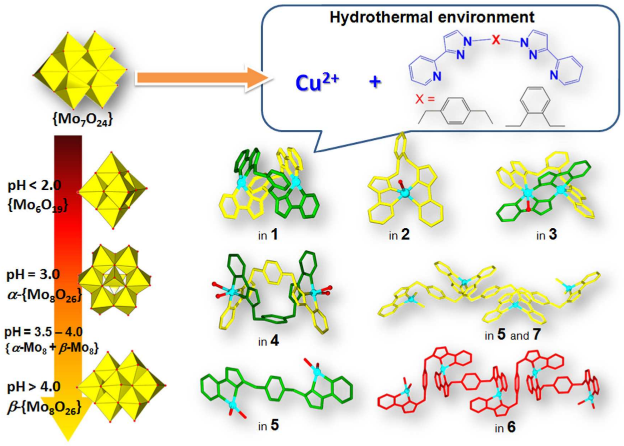

Scheme 2 Schematic view of the *in situ* structural transformation of heptamolybdate at different pH and the POMs act as "molecular adaptor" to modulate the metal-organic secondary building units in the hydrothermal envrionment.

Photocatalytic properties

The use of photocatalysts to decompose waste organic molecules so as to purify the water resources are of great interest for scientific research and the important concerned issue for our society. In this research field, Rhodamine-B (RhB) is generally employed as a typical model dye contaminant to evaluate the photocatalytic effectiveness in the purification of waste water.[13] POMs have been proved as one type of potential photocatalysts in the degradations of organic dyes.[14] However, the typical POM salts are usually water-soluble and may induce the secondary pollution if they are directly used as photocatalysts for the above purpose. Therefore, exploring heterogeneous POM-based photocatalysts are one of key issues in this research field. POM-based inorganic-organic hybrid compounds prepared in the hydrothermal or solvothermal environments usually show a very low solubility or even insolubility in water, which reveals an ideal route to develop new photocatalysts for the degradations of organic dyes in aqueous media.[15] Herein, all seven compounds are insoluble in water, and therefore their heterogeneous photocatalytic performances were investigated via the experimental model of RhB photodegradation under UV irradiation. Moreover, the photocatalytic property of the blank RhB aqueous solution without any catalyst was also checked as the control experiments. The RhB solutions were monitored by UV-vis spectra and the decolorization speeds under different conditions are displayed in Fig. 12. The absorption peaks of RhB solution decreased obviously under UV irradiation for compounds **1-7** and the photodegradation process of RhB without any photocatalyst have also been studied for comparison. Changes in C_t/C_0 plot of RhB solutions versus reaction time were shown in Fig. 12h. It is observed that the photocatalytic activities increase from 35.8% (without catalysts) to 83.9% for **1**, 82.3% for **2**, 84.0% for **3**, 84.5% for **4**, 81.5% for **5**, 80.0% for **6** and 79.0% for **7** after 90 min of irradiation. Compared with RhB without any photocatalyst, the absorption peak of compounds **1-7** decreased obviously upon irradiation, indicating that these compounds have good photocatalysis properties degradation of RhB. Moreover, since compound **4** exhibits the highest catalytic activity, it is further chosen as the representive catalyst to investigate the catalyst lifetime. In our initial experiment, the catalytic activity of compound **4** can be well sustained when it was recycled for five times (Fig. S22). Furthermore, PXRD pattern of compound **4** after five-cycle photocatalytic tests is still correspondence with the one before catalytic test, indicating that such heterogeneous catalysts are stable during the catalytic process (Fig. 13).

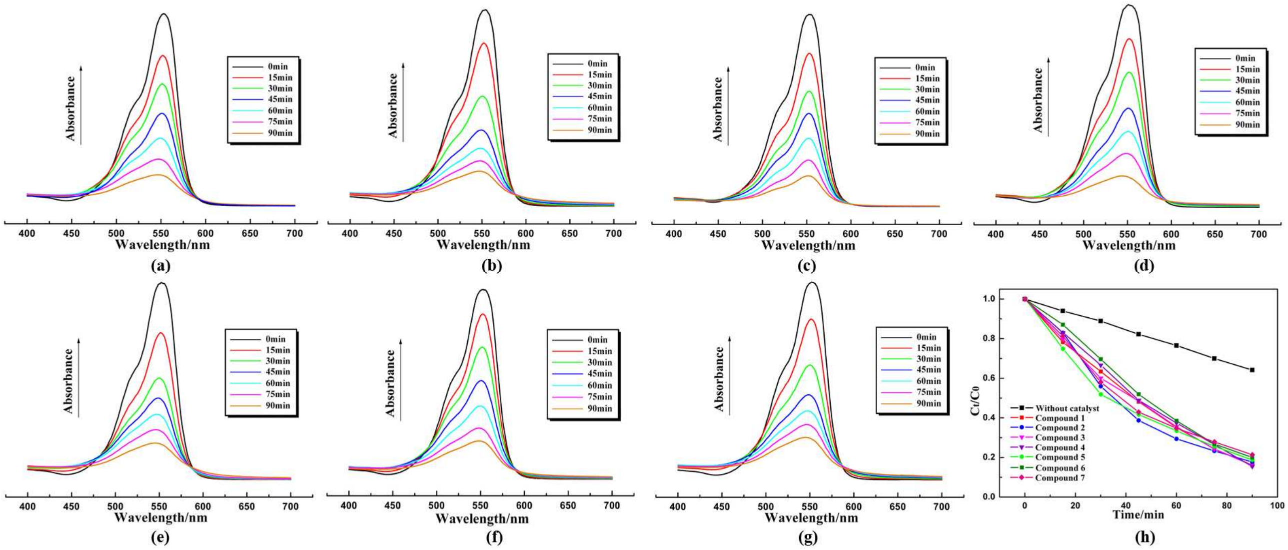

(a) (b) (c) (d) (e) (f) (g) (h)

Figure 12 (a–g) UV–vis absorption spectra of the RhB solution during the decomposition reaction under UV light irradiation in the presence of **compound 1-7**, respectively; **(h)** Plot of irradiation time versus concentration for RhB under UV light in the presence of the **compound 1-7**, and the black curve is the control experiment without any catalyst.

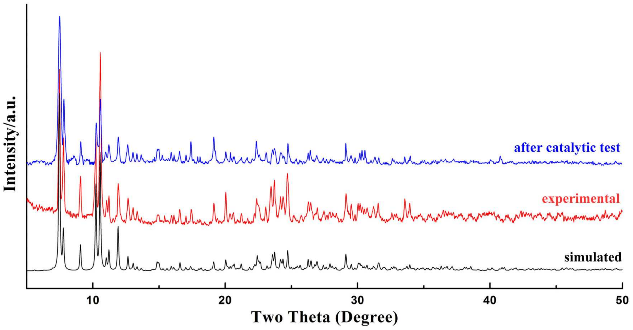

Figure 13 Simulated (black), experimental (red) and recovered after catalytic test (purple) XRD patterns of compound **4**.

Luminescent properties

The luminescent properties of compounds **1–7** have also been explored, considering that the organic ligands may induce the luminescent behaviors. Actually, upon excitation at 260 nm, intense emission peak of compounds **1-3** are located at 373 nm, 376 nm and 375 nm, respectively (Fig. 14a) and can be assigned to organic ligand-based emission (λ_{em}=363nm) according to the luminescence spectrum of the free L*o* ligand (Fig. 14a). Meanwhile, the emission peak positions at ca. 384 nm, 378 nm, 380 nm and 392 nm for compounds **4-7** are similar to that of **1-3** (Fig. 14b)**,** which are attributed to organic ligand-based emission (λ_{em}=365nm) according to the luminescence spectrum of the free L*p* ligand (Fig. 14b). This emission band can be ascribed to a π-π* or π-n ligand-centered electronic transition within the aromatic systems of the L ligand.[16]

Conclusions

In summary, seven new organic–inorganic hybrid compounds based on the TM ions, bichelate-bridging ligands and polyoxomolybdate units have been prepared. In such a reaction system, the heptamolybdate $[Mo_7O_{24}]^{6-}$ can *in situ* transform to hexamolybdate or octamolybdate by changing pH. These POM clusters can be viewed as a "molecular adaptor" to tune the appropriate form of metal-organic subunits, such as the "Möbius ring"-type binuclear unit, "S"-type binuclear unit, butterfly-type unit, helical chain and mesomeric helical chain. As a result, these POM anions and various metal-organic subunits have the best matching mode in the self-assembly process, leading to new hybrid compound system. These POM-based hybrid materials display good photocatalytic activities towards the model degradation experiment of RhB under UV irradiation. Based on the present work, it can be predicted that the use of a dynamic configuration of POM anions to modulate the metal-organic coordination complex moieties may be developed as a new strategy to design and synthesis of hybrid compound systems with desirable structures and functionalities in the future. This work is ongoing in our group.

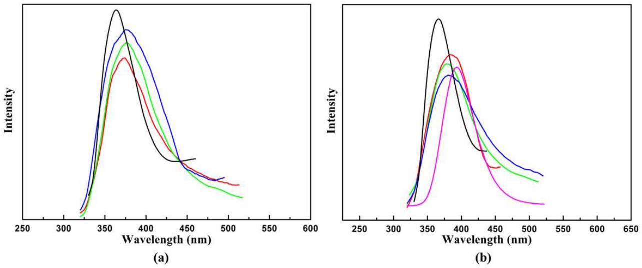

Figure 14 (a) Emission spectra of free L*o* (black) excited at 325 nm and emission spectra of compound **1** (red), **2** (green) and **3** (blue) excited at 260 nm; **(b)** Emission spectra of free L*p* (black) excited at 325 nm and emission spectra of compound **4** (red), **5** (green), **6** (blue) and **7** (magenta) excited at 260 nm.

Acknowledgments

This work was supported by National Natural Science Foundation of China (grant nos. 21271039, 21201032), Program for New Century Excellent Talents in University (grant no. NCET120813) and Fundamental Research Funds for the Central Universities (grant no. 11SSXT140).

Notes and references

[a] *Key Laboratory of Polyoxometalate Science of Ministry of Education, Department of Chemistry, Northeast Normal University, Changchun, 130024, P. R. China*
E-mail: zanghy100@nenu.edu.cn (H.-Y. Zang) and liyg658@nenu.edu.cn (Y.-G. Li)
[b] *School of Chemical and Biological Engineering, Tai Yuan Science and Technology University, Taiyuan 030012, PR China*

† Electronic Supplementary Information (ESI) available: Summary of selected bond lengths and angles; IR, TG and PXRD and cif files of **1**-**7**. CCDC reference numbers: 947642 (1), 947643 (2), 947644 (3), 947645 (4), 947646 (5), 947647 (6) and 947641 (7). See DOI: 10.1039/b000000x/

1. (a) P. Huang, C. Qin, Z. M. Su, Y. Xing, X. L. Wang, K. Z. Shao, Y. Q. Lan and E. B. Wang, *J. Am. Chem. Soc.*, 2012, **134**, 14004; (b) S. J. Li, S. M. Liu, S. X. Liu, Y. W. Liu, Q. Tang, Z. Shi, S. X. Ouyang and J. H. Ye, *J. Am. Chem. Soc.*, 2012, **134**, 19716; (c) O. Oms, A. Dolbecq and P. Mialane, *Chem. Soc. Rev.*, 2012, **41**, 7497; (d) K. Uehara, K. Fukaya and N. Mizuno, *Angew. Chem. Int. Ed.*, 2012, **51**, 7715; (e) A. B. S. Banerjee, G. V. Röschenthaler and U. Kortz, *Chem. Soc. Rev.*, 2012, **41**, 7590; (f) X. J. Feng, Y. G. Li, Z. M. Zhang and E. B. Wang, *Acta Chim. Sinica.*, 2013, **71**, 1575; (g) X. L. Hao, M. F. Luo, W. Yao, Y. G. Li, Y. H. Wang and E. B. Wang, *Dalton Trans.*, 2011, **40**, 5971; (h) H. N. Miras, J. Yan, D. L. Long and L. Cronin, *Chem. Soc. Rev.*, 2012, **41**, 7403.
2. (a) F. J. Ma, S. X. Liu, C. Y. Sun, D. D. Liang, G. J. Ren, F. Wei, Y. G. Chen and Z. M. Su, *J. Am. Chem. Soc.*, 2011, **133**, 4178; (b) B. Nohra, H. El Moll, A. Rodriguez, L. M. Mialane, P. J. Marrot, C. Mellot-Draznieks, M. O'Keeffe, J. Biboum, R. N. Lemaire, B. Keita, L. Nadjo and A. Dolbecq, *J. Am. Chem. Soc*., 2011, **133**, 13363; (c) C. Zou, Z. J. Zhang, X. Xu, Q. H. Gong, J. Li and C. D. Wu, *J. Am. Chem. Soc.*, 2012, **134**, 87; (d) H. J. Pang, J. Peng, C. J. Zhang, Y. G. Li, P. P. Zhang, H. Y. Ma and Z. M. Su, *Chem. Commun.*, 2010, **46**, 5097; (e) B. Liu, J. Yang, G. C. Yang and J. F. Ma, *Inorg. Chem.*, 2013, **52**, 84.
3. (a) X. L. Hao, Y. Y. Ma, C. Zhang, Q. Wang, X. Cheng, Y. H. Wang, Y. G. Li and E. B. Wang, *CrystEngComm.*, 2012**, 14**, 6573; (b) X. L. Hao, Y. Y. Ma, Y. H. Wang, L. Y. Xu, F. C. Liu, M. M. Zhang and Y. G. Li, *Chem. Asian J.*, 2014, **9**, 819.
4. (a) H. Fu, C. Qin, Y. Lu, Z. M. Zhang, Y. G. Li, Z. M. Su, W. L. Li and E. B.Wang, *Angew. Chem. Int. Ed.*, 2012, **51**, 7985; (b) J. X. Meng, Y. Lu, Y. G. Li, H. Fu and E. B. Wang, *CrystEngComm.*, 2011, **13**, 2479; (c) Z. Zhang, J. Yang**,** Y. Y. Liu and J. F. Ma, *CrystEngComm.*, 2013, **15**, 3843; (d) H. Fu, Y. Lu, Z. L. Wang, C. Liang, Z. M. Zhang and E. B. Wang, *Dalton Trans.*, 2012, **41**, 4084.
5. (a) D. G. Allis, R. S. Rarig, E. Burkholder and J. Zubieta, *J. Mol. Struct.*, 2004, **688**, 11; (b) P. J. Hagrman and J. Zubieta, *Inorg. Chem.*, 1999, **38**, 4480.
6. (a) Y. Wang, Y. Peng, L. N. Xiao, Y. Y. Hu, L. M. Wang, Z. M. Gao, T. G. Wang, F. Q. Wu, X. B. Cui and J. Q.Xu, *CrystEngComm.*, 2012, **14**, 1049; (b) M. Yuan, Y. G. Li, E. B. Wang, C. G. Tian, L. Wang, C. W. Hu, N. H. Hu and H. Q. Jia, *Inorg. Chem.*, 2003, **42**, 3670; (c) L. M. Dai, W. S. You, Y. G. Li, E. B. Wang and C. Y. Huang, *Chem. Commun*., 2009, 2721; (d) G. Y. Luan, Y. G. Li, S. T. Wang, E. B. Wang, Z. B. Han, C. W. Hu, N. H. Hu and H. Q. Jia, *J. Chem. Soc. Dalton Trans*., 2003, 233.
7. (a) J. Q. Sha, J. W. Sun, M. T. Li, C. Wang, G. M. Li, P. F. Yan and L. J. Sun, *Dalton Trans*., 2013, **42**, 1667; (b) A. X. Tian, J. Ying, J. Peng, J. Q. Sha, H. J. Pang, P. P. Zhang, Y. Chen, M. Zhu and Z. M. Su, *Inorg. Chem*. 2009, **48**, 100; (c) X. L. Wang, J. Li, A. X. Tian, G. C. Liu, Q. Gao, H. Y. Lin, D. Zhao, *CrystEngComm*., 2011, **13**, 2194.
8. (a) X. Wang, M. M. Zhang, X. L. Hao, Y. H. Wang, Y. Wei, F. S. Liang, L. J. Xu and Y. G. Li, *Cryst. Growth Des*., 2013, **13**, 3454; (b) M. M. Zhang, X. L. Hao, L. J. Xu, Y. H. Wang, X. Wang, Y. G. Li, *Journal of Solid State Chemistry*., 2014, **215**, 57.
9. (a) J. S. Fleming, K. L. V. Mann, C. A. Carraz, E. Psillakis, J. C. Jeffery, J. A. McCleverty and M. D. Ward, *Angew. Chem. Int. Ed*., 1998, **37**, 1279; (b) A. J. Amoroso, A. M. C. Thompson, J. C. Jeffery, P. L. Jones, J. A. McCleverty and M. D. Ward, *J. Chem. Soc., Chem. Commun*., 1994, 2751.
10. (a) G. M. Sheldrick, SHELXS97, Program for Crystal Structure Solution, University of Göttingen: Göttingen, Germany, 1997; (b) G. M. Sheldrick, SHELXL97, Program for Crystal Structure Refinement, University of Göttingen: Göttingen, Germany, 1997.
11. A. L. Spek, PLATON, A Multipurpose Crystallographic Tool; Utrecht University: Utrecht, The Netherlands, 1998.
12. C. Qin, X. L. Wang, L. Yuan and E. B. Wang, *Cryst. Growth Des.*, 2008, **8**, 2093.
13. (a) Q. Wang, C. C. Chen, D. Zhao, W. H. Ma and J. C. Zhao, *Langmuir,* 2008, **24**, 7338; (b) C. C. Chen, W. Zhao, P. X. Lei, J. C. Zhao and N. Serpone, *Chem.Eur. J.,* 2004, **10***,* 1956.
14. (a) A. Troupis, T. M. Triantis and E. Gkika, *Applied Catal. B,* 2009, **86**, 98; (b) I. Arslan-Alaton, *Dyes and Pigments*, 2003, **60**, 167; (c) Y. Yang, Q. Y. Wu, Y. H. Guo, C. W. Hu and E. B. Wang, *J. Mol. Catal. A,* 2005, **225**, 203.
15. (a) H. Y. Liu, H. Wu, J. F. Ma, Y. Y. Liu, J. Yang and J. C. Ma, *Dalton Trans*., 2011, **40**, 602; (b) Y. Q. Chen, G. R. Li, Y. K. Qu, Y.

H. Zhang, K. H. He, Q. Gao and X. H. Bu, *Cryst. Growth Des.*, 2013, **13**, 901.

16. (a) F. Y. Yi, N. Zhao, W. Wu and J. G. Mao, *Inorg. Chem.*, 2009, **48**, 628; (b) B. Xu, J. Lü and R. Cao, *Cryst. Growth Des.*, 2009, **9**, 3003; (c) Y. W. Li, J. R. Li, L. F. Wang, B. Y. Zhou, Q. Chen and X. H. Bu, *J. Mater. Chem. A*, 2013, **1**, 495.

Graphical Abstract

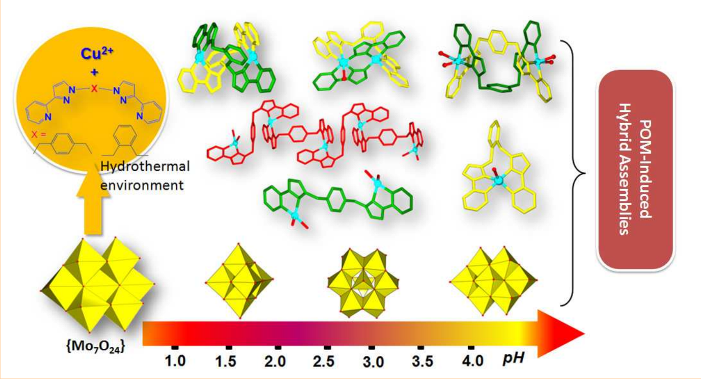

The heptamolybdate shows various structural transformation in different pH, which is used as a "molecular adaptor" to modulate the metal-organic coordination building units in the hydrothermal environment, leading to the isolation of new polyoxometalate-induced hybrid assemblies with good photocatalytic activity.